Satellite Detection of Orographic Gravity-Wave Activity in the Winter Subtropical Stratosphere over Australia and Africa

S. D. Eckermann,[1], and D. L. Wu,[2]

S. D. Eckermann, Space Science Division, Code 7631, Naval Research Laboratory, 4555 Overlook Ave. SW, Washington, DC 20375, USA. (stephen.eckermann@nrl.navy.mil)

[1]Space Science Division, Naval Research Laboratory, Washington, DC, USA.

[2]NASA Goddard Space Flight Center, Greenbelt, Maryland, USA.

Orographic gravity-wave (OGW) parameterizations in models produce waves over subtropical mountain ranges in Australia and Africa that propagate into the stratosphere during austral winter and deposit momentum, affecting weather and climate. Satellite sensors have measured stratospheric GWs for over a decade, yet find no evidence of these waves. So are parameterizations failing here? Here we argue that the short wavelengths of subtropical OGWs place them near or below the detection limits of satellite sensors. To test this hypothesis, we reanalyze nine years of stratospheric radiances from the Atmospheric Infrared Sounder (AIRS) on NASA's Aqua satellite during austral winter, applying new averaging techniques to maximize signal-to-noise and improve thresholds for OGW detection. Deep climatological enhancements in stratospheric OGW variance over specific mountain ranges in Australia and southern Africa are revealed for the first time, which exhibit temporal and vertical variations consistent with predicted OGW responses to varying background winds.

1. Introduction

High-resolution high-precision stratospheric radiances from limb and nadir satellite sensors can resolve temperature perturbations produced by long-wavelength gravity waves (GWs), providing insights into the global distribution of stratospheric GW activity [*Wu et al.*, 2006]. In austral winter, climatologies reveal a band of enhanced variance at ∼40-70°S, punctuated by localized "hot spots" due to deep stratospheric propagation of orographic gravity waves (OGWs) from major mountain ranges, such as the southern Andes, southern Alps, and coastal Antarctic mountain ranges [e.g., *Eckermann and Preusse*, 1999; *McLandress et al.*, 2000; *Wu*, 2004; *Jiang et al.*, 2005; *Wu and Eckermann*, 2008; *Alexander et al.*, 2008; *Yan et al.*, 2010; *Gong et al.*, 2012], as well as from small mountainous islands scattered along the Southern Ocean [*Wu et al.*, 2006; *Alexander et al.*, 2009].

Conversely, in the southern winter subtropics (25°–40°S), satellite sensors detect few deep stratospheric orographic gravity waves (SOGWs), despite the presence of greater and more significant orography at these latitudes. While satellite sensors regularly detect SOGWs over the subtropical Andes [*Jiang et al.*, 2002; *Wu*, 2004], significant subtropical orography in Africa and mainland Australia yields no clear SOGW signatures. Why?

The simplest explanation is that there are no waves to observe. On moving equatorward, prevailing mid-latitude westerlies near the surface and throughout the stratosphere weaken significantly and eventually reverse, reducing surface forcing and inhibiting SOGW penetration through critical-level filtering and wave breaking in the lower stratosphere. Yet deep mountain-wave hindcasting by *Jiang et al.* [2005] has shown that these effects alone do not prevent deep climatological SOGW signatures from occurring over subtropi-

cal Australian and African orography in austral winter. Parameterizations in weather and climate models also predict significant deposition of SOGW momentum in the southern winter subtropics [e.g., *Scinocca and McFarlane*, 2000].

While this discepansy could of course point to model shortcomings, another possibility is an inability of satellites sensors to detect these SOGWs. Subtropical Australian and African mountain ranges are lower and narrower than the subtropical Andes, forcing OGWs with shorter horizontal wavelengths λ_h and smaller amplitudes. OGW vertical wavelengths λ_z are proportional to local wind speeds U, and both reduce considerably on moving from midlatitudes to subtropics [*Jiang et al.*, 2002]. The anticipated small amplitude and short wavelengths of these waves means that their signals in nadir and limb radiances will be weak, and possibly too weak to exceed channel noise floors.

Here we undertake a systematic reanalysis of GW perturbations in stratospheric thermal radiances from the Atmospheric Infrared Sounder (AIRS) on NASA's polar-orbiting Aqua satellite, employing a range of averaging procedures to yield radiance scenes with reduced background noise levels. The objective is to see whether statistically significant signatures of subtopical SOGWs, previously buried within the noise, emerge over Australia and Africa in austral winter.

2. Noise-Reduced Gravity-Wave Signals from AIRS Radiances

AIRS is a passive infrared sensor that scans the atmosphere perpendicular to the satellite track in a repeating series of 90 measurements distributed symmetrically about the nadir. Areas of individual measurement footprints range from ∼13x13 km^2 at nadir to ∼31x21 km^2 at the far off-nadir. As Aqua orbits, AIRS sweeps out pole-to-pole measure-

ment swaths ∼1650 km wide, accumulating radiances from over 2300 channels, most of which are tropospheric but many of which peak in the stratosphere. While the contribution functions for these radiances are vertically broad, the high radiometric precision and low noise levels of individual channels, coupled with small measurement footprints, allow temperature perturbations of deep (long λ_z) GWs to be resolved as horizontal two-dimensional wave structure in the pushbroom radiance imagery from many stratospheric channels.

From 100-20 hPa there are redundant AIRS thermal channels that peak at nearly the same altitude with very similar vertical weighting functions. Following *Eckermann et al.* [2009] and *Gong et al.* [2012], we averaged version 5 radiances from 50 AIRS channels to produce a mean radiance product at 12 pressure levels from 100-2 hPa [see Table A2 of *Gong et al.*, 2012]. At the lowest levels of 100 hPa, 80 hPa and 60 hPa, where we most require reduced noise for better GW detection near the source, the product was derived by averaging radiances from 6, 14 and 9 individual AIRS channels, respectively.

Occasionally these data revealed outbreaks of anomalous radiance at specific scan angles, often prior to extended periods of missing data. This striping prevents a clean isolation of small-scale GW perturbations and contaminates variance maps, so daily radiance maps from 2003-2011 were carefully screened to identify and remove errant granules.

GW perturbations were isolated by fitting and removing large-scale radiance structure, as follows. Swath radiances were first smoothed along track using a 33-point running average (∼660 km), then each scan was fitted cross track using a sixth-order polynomial, to capture both geophysical cross-track gradients as well as systematic scan-angle trends

due to the limb effect. These smoothed fields were subjected to a final 15-point along-track running average, then subtracted from the original radiances to isolate small-scale perturbation structure. The radiance perturbation maps were smoothed using a 3x3 point running average to reduce random noise levels still further. Perturbation variances at each level were computed and stored daily on a global 0.5°x1° longitude-latitude grid.

3. Subtropical SOGWs over Australia

Figure 1a plots topographic elevations over southern Australia. Remaining panels show root-mean-square (rms) GW-induced brightness temperature perturbations, $\hat{T}_{rms}$, at altitudes from 100 hPa up to 2 hPa, averaged throughout austral winter (June-August) for the years 2003-2011. This nine-year climatology reveals for the first time clear "hot spots" of SOGW activity in the lower stratosphere from 100-60 hPa (Figure 1b–1d) associated with major Australian mountain ranges labeled in Figure 1a: the Great Dividing Range on the east coast, and the Flinders Ranges in southern Australia to the north of Adelaide. The improved signal-to-noise levels even reveal a weak but distinct SOGW signal on the southwest coast associated with the Darling Ranges, a comparitively low mountain escarpment running along the west Australian coast near Perth. A noteable feature of all three SOGW-generating mountain ranges is their two-dimensional structure and north-south alignment, which, like the Andes, is favorable for strong surface OGW forcing and deep stratospheric propagation within a prevailing westerly winter flow at all altitudes. A fourth (midlatitude) SOGW enhancement is evident at 100–60 hPa over Tasmania.

On progressing deeper into the stratosphere, $\hat{T}_{rms}$ maps develop a band of elevated values poleward of 40°S. This results from intensifying stratospheric westerlies that refract

nonorographic GWs at these latitudes to long λ_z values, making them easier for AIRS to resolve and producing larger radiance signals. Nonetheless, the largest $\hat{T}_{rms}$ values at these latitudes are still associated with SOGWs from Tasmania, as has been noted in some earlier studies [*Wu*, 2004; *Jiang et al.*, 2005]. Despite the dominance of these midlatitude GW radiance signals at upper levels, the $\hat{T}_{rms}$ maps continue to show local SOGW maxima over the Great Dividing Range, Flinders Ranges, and even (weakly) over the Darling Range all the way up to 2 hPa (Figure 1e), consistent with deep propagation of these subtropical SOGWs.

Boxes in Figure 2a demark these four regions of SOGW activity, within which daily $\hat{T}_{rms}$ values are computed. Figure 3 plots resulting daily time series of $\hat{T}_{rms}$ at three different altitudes. In the lower stratosphere at ∼80 hPa (bottom row of Figure 3), the time series reveal sporadic generation of waves throughout May-September, with a weak tendency for greater activity in winter. The largest values occur over the Great Dividing Range, consistent with Figure 1c. By contrast, $\hat{T}_{rms}$ time series at 7 hPa and 2 hPa reveal largest values over Tasmania, mostly confined to the austral winter months of June-August, whereas values over the three subtropical SOGW regions in mainland Australia are weaker and enhancements are restricted to June and July only.

To investigate the origins of this upper-level variability, Figures 2b and 2c show time series of zonal winds at 32°S and 43°S, respectively, over a limited range of Australian longitudes, depicted with broken gray curves in Figure 2a. These plots reveal stronger upper-level westerlies over Tasmania relative to mainland Australia, which refract Tasmanian SOGWs to longer λ_z values. These longer Tasmanian SOGWs are easier for AIRS to

detect than shorter subtropical SOGWs over mainland Australia, explaining their larger radiance signals from ∼20–2 hPa. By contrast, at ∼80 hPa, where wind speeds are more comparable at both latitudes, Tasmanian SOGW signals no longer dominate,

Shaded regions in Figures 2b and 2c show times when and altitudes where mean zonal winds are less than +5 m s^{-1}. It is difficult for SOGWs to propagate through these shaded regions to higher altitudes, due to critical-level removal or significant dissipation of wave energy due to wave breaking. Figure 2b reveals only a two month window in June and July at 32°S where these weak or reversed winds are absent and provide a favorable propagation channel to upper altitudes, consistent with observations in Figure 3 showing upper-level $\hat{T}_{rms}$ enhancements over mainland Australia confined to June and July. Figure 2c shows that at 43°S, this window expands into August, consistent with enhanced upper-level $\hat{T}_{rms}$ values over Tasmania in Figures 3j and 3k from June through August.

4. Subtropical SOGWs over southern Africa

We have applied the same analysis to search for subtropical SOGW signals over southern regions of Africa. Like Australia, AIRS radiances from 100-60 hPa reveal isolated hot spots in Figures 4b–4d associated with SOGWs generated by local mountain ranges evident in Figure 4a: the Drakensberg Mountains and Cape Fold Belt in South Africa and the Huns and Karas Mountains in Namibia. As in the Australian sector, on progressing upwards the $\hat{T}_{rms}$ maps acquire a belt of elevated values over the Southern Ocean. Nonetheless, the upper-level $\hat{T}_{rms}$ maps still show local subtropical maxima over the land masses relative to ocean regions to the east and west. While not as clear as over mainland Australia,

these observations nevertheless show that these subtropical SOGWs over South Africa and Namibia propagate deep into the upper stratosphere.

5. Summary

This study has resolved a discrepansy between models and observations by showing for the first time that subtropical mountain ranges in Australia and Africa generate OGWs that can be observed propagating deep into the stratosphere during austral winter. These waves had previously evaded satellite detection due to their short wavelengths, which place them at the resolution limits of limb and nadir sensors. Despite their small observed radiance signals, this deep subtropical SOGW activity is dynamically important, since parameterizations predict significant deposition of SOGW momentum in the southern subtropical lower stratosphere during austral winter [*Scinocca and McFarlane*, 2000], which in turn impacts large-scale weather and climate.

We found no clear SOGW signals equatorward of ∼25°S over Australia or Africa in austral winter. While even shorter SOGWs may exist here that continue to evade satellite detection, at these lower latitudes zero-wind lines form at ∼30 hPa over the Australian and African sectors which likely absorb many SOGWs via critical-level interactions.

Acknowledgments. This work was partially supported by NASA through the NRA NNH09ZDA001N-TERRAQUA (The Science of Terra and Aqua), grant NNH11AQ99I.

References

Alexander, M. J., et al. (2008), Global estimates of gravity wave momentum flux from High Resolution Dynamics Limb Sounder observations, *J. Geophys. Res.*, *113*, D15S18,

doi:10.1029/2007JD008807.

Alexander, M. J., S. D. Eckermann, D. Broutman and J. Ma (2009), Momentum flux estimates for South Georgia Island mountain waves in the stratosphere observed via satellite, *Geophys. Res. Lett.*, *36*, L12816, doi:10.1029/2009GL038587.

Eckermann, S. D. and P. Preusse (1999), Global measurements of stratospheric mountain waves from space, *Science*, *286*, 1534-1537.

Eckermann, S. D., L. Hoffmann, M. Höpfner, D. L. Wu and M. J. Alexander (2009), Antarctic NAT PSC belt of June 2003: Observational validation of the mountain wave seeding hypothesis, *Geophys. Res. Lett.*, *36*, L02807, doi:10.1029/2008GL036629.

Gong, J., D. L. Wu, and S. D. Eckermann (2012), Gravity wave variances and propagation derived from AIRS radiances, *Atmos. Chem. Phys.*, *12*, 1701-1720.

Jiang, J. H., D. L. Wu, and S. D. Eckermann (2002), Upper Atmosphere Research Satellite (UARS) MLS observation of mountain waves over the Andes, *J. Geophys. Res.*, *107*(D20), 10.1029/2002JD002091.

Jiang, J. H., S. D. Eckermann, D. L. Wu, K. Hocke, B. Wang, J. Ma, and Y. Zhang (2005), Seasonal variation of gravity wave sources from satellite observation, *Adv. Space Res.*, *35*, 1925-1932.

McLandress, C., M. J. Alexander, and D. L. Wu (2000), Microwave Limb Sounder observations of gravity waves in the stratosphere: A climatology and interpretation, *J. Geophys. Res.*, *105*(D9), 11,947-11,967.

Preusse, P., et al. (2006), Tropopause to mesopause gravity waves in August: Measurement and modeling, *J. Atmos. Sol.-Terr. Phys.*, *68*, 1730-1751.

187 Rienecker, M. M., et al. (2011), MERRA: NASA's modern-era retrospective analysis for
188 research and applications, *J. Climate*, *24*, 3624-3648.

189 Scinocca, J. F. and N. A. McFarlane (2000), The parameterization of drag induced by
190 stratified flow over anisotropic orography, *Quart. J. Roy. Meteor. Soc.*, *126*, 2353-2393.

191 Wu, D. L. (2004), Mesoscale gravity wave variances from AMSU-A radiances, *Geophys.*
192 *Res. Lett.*, *31*, L12114, doi:10.1029/2004GL019562.

193 Wu, D. L., and S. D. Eckermann (2008), Global gravity wave variances from Aura MLS:
194 Characteristics and interpretation, *J. Atmos. Sci.*, *65*, 3695-3718.

195 Wu, D. L., P. Preusse, S. D. Eckermann, J. H. Jiang, M. de la Torre Juarez, L. Coy, and
196 D. Y. Wang (2006), Remote sounding of atmospheric gravity waves with satellite limb
197 and nadir techniques, *Adv. Space Res.*, *37*, 2269-2277.

198 Yan, X., N. Arnold, and J. Remedios (2010), Global observations of gravity waves
199 from High Resolution Dynamics Limb Sounder temperature measurements: A year-
200 long record of temperature amplitude and vertical wavelength, *J. Geophys. Res.*, *115*,
201 D10113, doi:10.1029/2008JD011511.

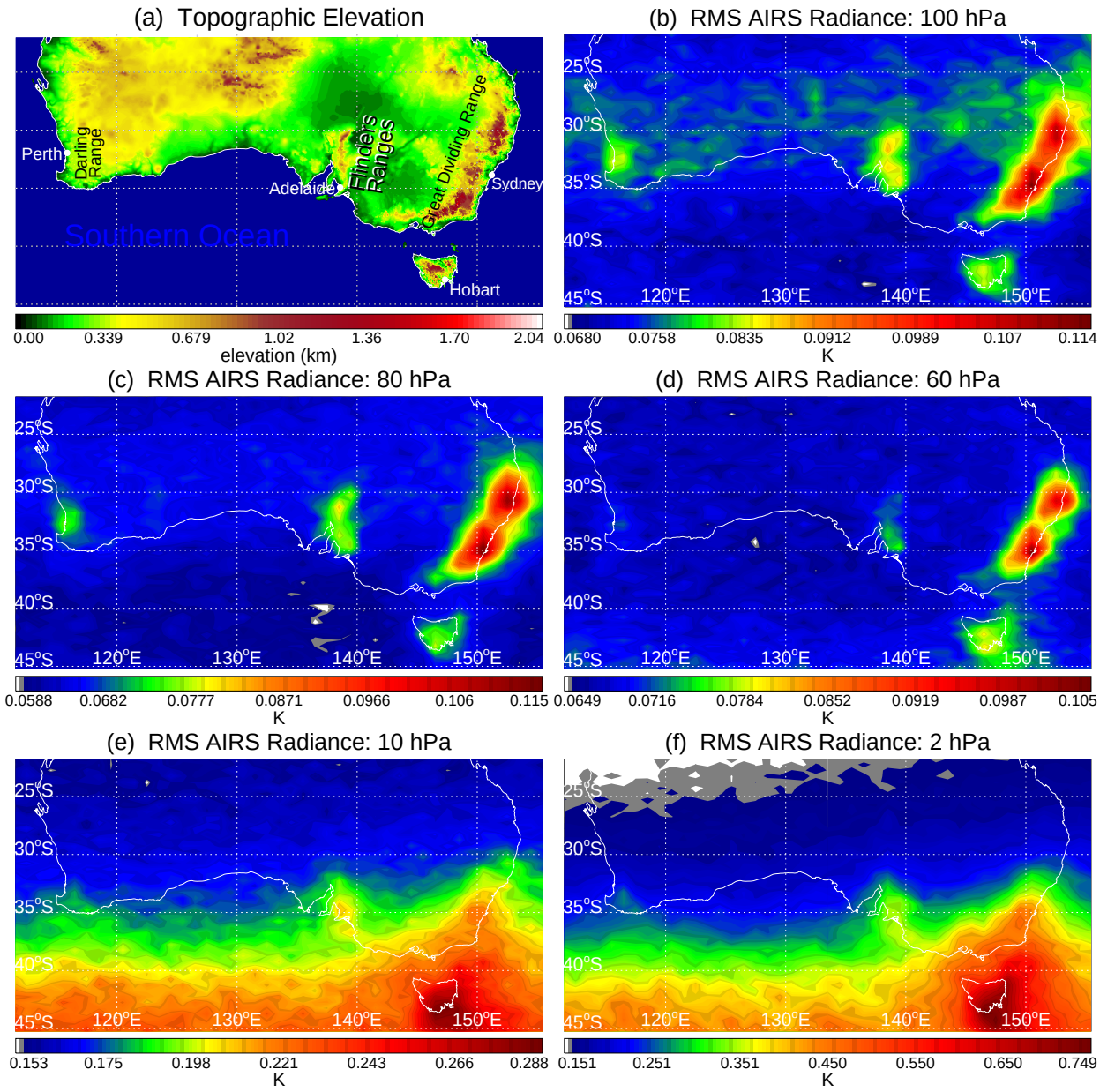

Figure 1. (a) Topographic elevations showing major mountain ranges over southern mainland Australia. Remaining panels show corresponding maps of rms SOGW-induced anomalies in AIRS brightness temperatures, $\hat{T}_{rms}$, averaged on a 0.5°x1° grid from June-August for the years 2003-2011, based on noise-reduced radiance imagery at (b) 100 hPa, (c) 80 hPa, (d) 60 hPa, (e) 10 hPa, and (f) 2 hPa.

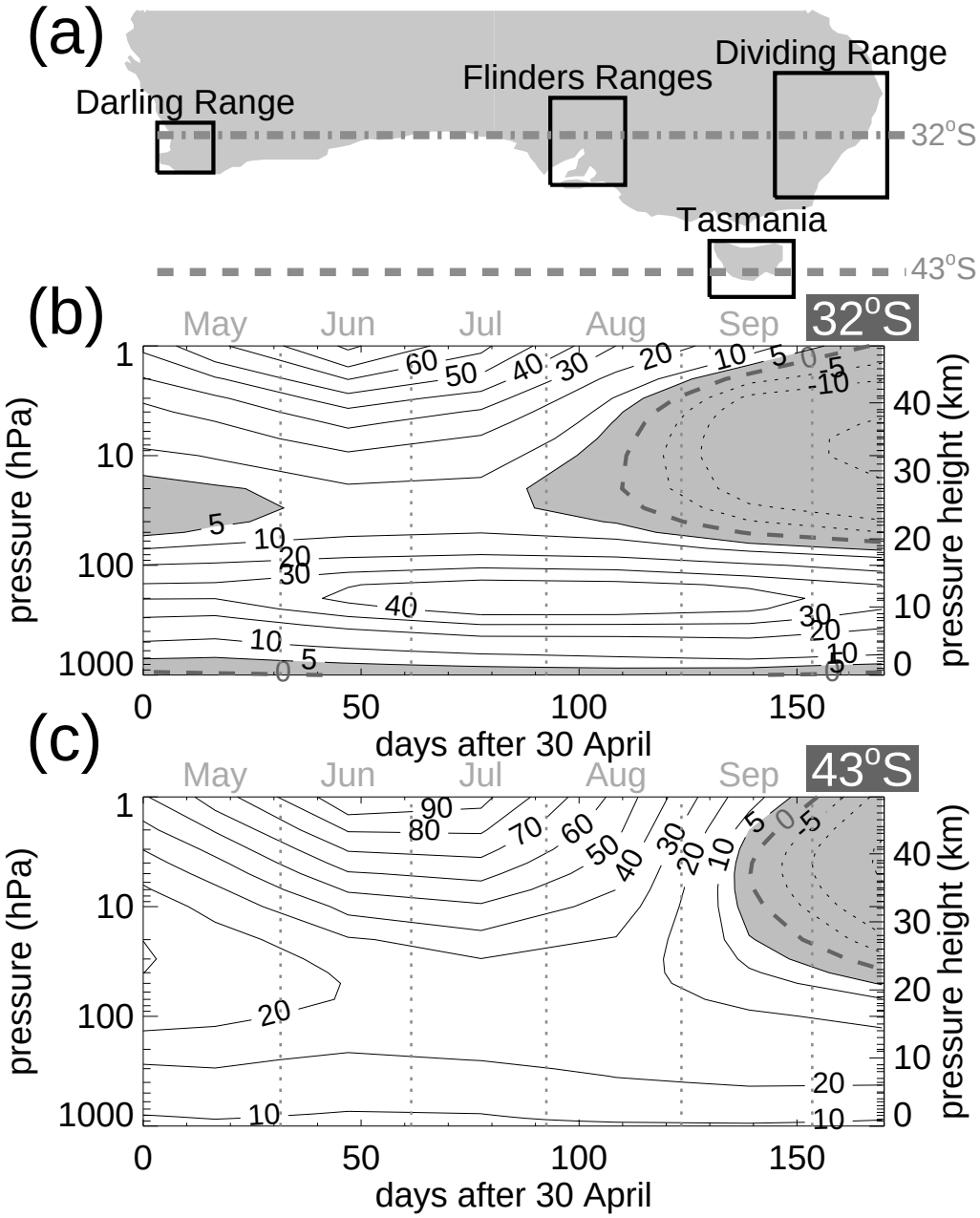

Figure 2. (a) Boxes show SOGW-active regions in Figure 1 that are used to compute $\hat{T}_{rms}$ time series in Figure 3. Broken gray lines show longitudinal regions at a given latitude where reanalysis zonal winds of *Rienecker et al.* [2011] are averaged from 2003–2011 and plotted versus time and height at (b) 32°S and (c) 43°S. Contour labels are in m s^{-1}, solid (dotted) contours depict westerlies (easterlies). Shaded regions denote winds $\leq$5 m s^{-1}.

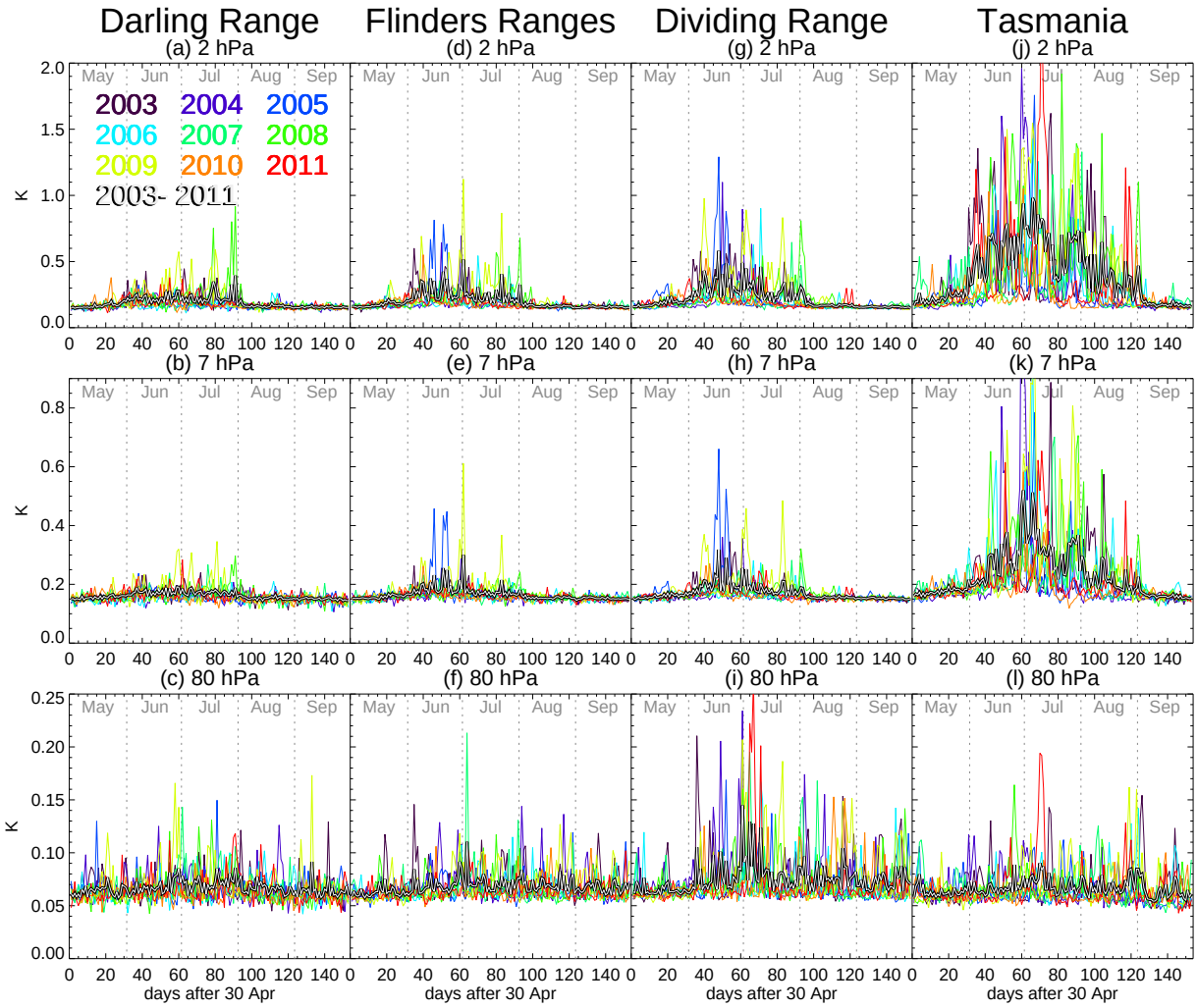

Figure 3. Daily time series of $\hat{T}_{rms}$ at 80 hPa (bottom row), 7 hPa (middle row) and 2 hPa (top row) from May-September within the four Australian SOGW regions identified in Figure 2a. Colored curves show time series for individual years (see color key in panel a), while the thick white-on-black curves show the nine-year mean.

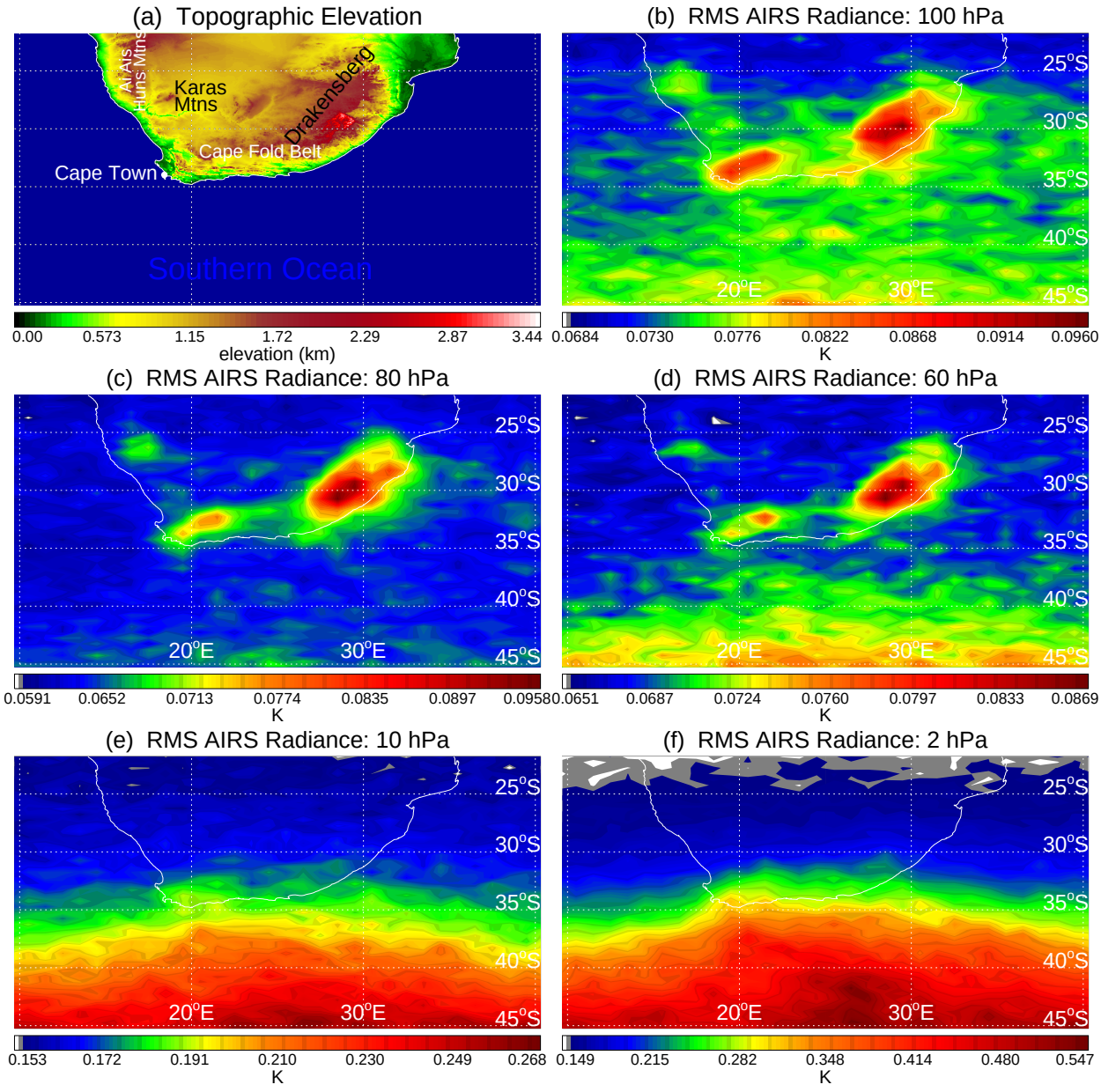

Figure 4. As for Figure 1, but focusing on the southern Africa region.